Available online at www.sciencedirect.com
ScienceDirect
Nuclear Instruments and Methods in Physics Research A 574 (2007) 324–329
NUCLEAR INSTRUMENTS & METHODS IN PHYSICS RESEARCH Section A
www.elsevier.com/locate/nima

Neutron refraction by cylindrical metal wires

J. Plomp[a,*], J.G. Barker[b], V.O. de Haan[a], W.G. Bouwman[a], A.A. van Well[a]

[a]*Faculty of Applied Sciences, Delft University of Technology, Delft, The Netherlands*
[b]*NIST Center for Neutron Research, National Institute of Standards and Technology, Gaithersburg, MD 20899, USA*

Received 8 December 2006; received in revised form 9 February 2007; accepted 12 February 2007
Available online 1 March 2007

Abstract

Undesired Small-Angle Neutron Scattering (SANS) from interior features of an object can be minimised by reducing the sample thickness. However, refraction effects produced by the exterior shape of the object depend upon the scattering cross-section and not on the thickness of the object. In the field of polarised neutrons a wire coil is often used to manipulate the polarisation vector of the neutron. In this paper, we show that the cylindrical shape of the wire together with the refractive index introduces an angular distribution in the neutron beam. This can be observed in instrumentation sensitive to SANS. We show results measured on three different SANS instruments: Ultra Small-Angle Neutrons Scattering (USANS), Spin-Echo Small-Angle Neutron Scattering (SESANS) and a Time-of-Flight (TOF) SESANS. These results are all in good agreement with the theory of refraction.

PACS: 03.75.Be; 61.12.Ex; 29.30.Hs

Keywords: USANS; SESANS; Neutron refraction; Coil; Spin-echo

1. Introduction

In Small-Angle Neutron Scattering (SANS) instruments it is hard and sometimes impossible to avoid placing objects in the beam, such as sample containers, windows or coils. To minimise the amount of small-angle scattering from these objects the thickness is minimised and a material with small scattering cross-section is chosen, such as aluminium (Al). However, refraction can also occur, even for thin objects. The shape of the object and scattering cross-section are the most important parameters determining the refraction.

Neutron refraction in a quartz prism was used already in 1982 by Gähler [1] to produce a monoenergetic cold neutron beam. At NIST refraction on biconcave lenses is used for focusing the beam in a SANS instrument for cold neutrons [2]. Refraction of thermal neutrons on an Al wedge was demonstrated by Rekveldt [3] with the technique of Spin-Echo Small-Angle Neutron Scattering (SESANS). The refraction angles for thermal neutrons on Al are typically in the order of micro-radians and are normally neglected. However, in Ultra Small-Angle Neutron Scattering (USANS), refraction is measurable. In SESANS with its expanding field of applications [4] it can significantly decrease the degree of "empty" beam polarisation of the instrument.

A common component in an instrument for polarised neutrons is a coil to manipulate the polarisation. Although such coils are preferably wound from Al wire (with small scattering cross-section) the cylindrical shape introduces neutron refraction perpendicular to the wire direction. We have measured this effect on three small-angle scattering instruments on which one can measure very small scattering angles. Two of them are based on the spin-echo method, i.e. the depolarisation of a polarised neutron beam is a measure for the change in angular distribution of the beam: (i) an instrument with a monochromatic beam of 0.21 nm wavelength, called as "monochromatic SESANS", and (ii) a prototype SESANS instrument, called as "TOF-SESANS" which operates in Time-of-Flight (TOF) mode in a polychromatic beam with a wavelength spectrum from 0.1 to

*Corresponding author. Tel.: +31 0 15 278 7109; fax: +31 0 15 2788303.
E-mail address: j.plomp@tudelft.nl (J. Plomp).

0168-9002/$ - see front matter © 2007 Elsevier B.V. All rights reserved.
doi:10.1016/j.nima.2007.02.068

0.65 nm [5,6]. This prototype is developed in Delft for implementation of the SESANS technique in the instrument "OffSpec" on the second target station at ISIS [7]. The third instrument is a ultra-high-resolution small-angle neutron scattering, USANS, a double-crystal diffractometer at the NIST Center for Neutron Research (NCNR) [8]. On this instrument one can measure very small wave vector transfers with high resolution in one (horizontal) direction; it uses a wavelength of 0.238 nm.

2. Theory

2.1. Refraction

If we describe the neutron as a wave we can understand and describe many observations with neutrons like diffraction, reflection and refraction [9]. One can introduce the refractive index for thermal neutrons

$$n = 1 - \delta \tag{1}$$

where the deviation from 1 is

$$\delta = \frac{\rho\lambda^2\bar{b}}{2\pi}. \tag{2}$$

Here ρ is the number of nuclei per unit volume, λ is the wavelength and $\bar{b}$ the mean coherent scattering length, which for most materials is positive, yielding a refraction index less than 1. This means that a cylinder will act as a lens with a negative focal length in a direction normal to the cylinder axis, while in the direction parallel to the wire, no change in direction will happen. Fig. 1 shows the geometry of a single cylindrical wire of radius, R, placed in a parallel neutron beam, with axis perpendicular to the beam direction. We use Snell's law of refraction,

$$\cos\alpha = \frac{Z}{R} = z$$
$$\cos\alpha = n\cos\beta \tag{3}$$

and we neglect the effect of absorption, caused by the imaginary part of δ.

The deviation between the incoming beam and outgoing beam $\vartheta = 2(\alpha-\beta)$. The angle α depends on the position Z of the trajectory on the wire. The deviation ϑ depends on the refractive index, n, and on α. After the beam has passed a layer of parallel wires, a distribution $I(\vartheta)$ of angles ϑ will be created. If the beam cross-section is 100% covered with a whole number of wires, this distribution does not depend on the number of wires. Also, the diameter of the wire is irrelevant for this distribution as long as the radius R is much larger than the coherence length of the neutron. Hence, we introduce the reduced beam position $z = Z/R$. Using Eqs. (1) and (3) we find for the deviation angle ϑ:

$$\sin\frac{\vartheta}{2} = \sqrt{1-z^2}\,\frac{z}{(1-\delta)} - z\sqrt{1-\frac{z^2}{(1-\delta)^2}}. \tag{4}$$

Since ϑ and δ are small we may write

$$\vartheta = \frac{2z}{\sqrt{1-z^2}}\delta. \tag{5}$$

With this equation and assuming a homogeneous beam we can implicitly write the distribution of deviation angles ϑ as

$$z = \frac{\vartheta}{\sqrt{4\delta^2+\vartheta^2}} \tag{6}$$

from which we find the normalised refractive angular distribution, $I(\vartheta)$, as observed in small-angle scattering

$$I(\vartheta) = \frac{\mathrm{d}z}{\mathrm{d}\vartheta}\Big/\int\frac{\mathrm{d}z}{\mathrm{d}\vartheta}\,\mathrm{d}\vartheta = \frac{1}{4\delta}\frac{1}{\left[1+(\vartheta/2\delta)^2\right]^{3/2}} \tag{7}$$

where we substituted the derivative of $I(\vartheta)$ on basis of Eq. (6)

$$\frac{\mathrm{d}z}{\mathrm{d}\vartheta} = \frac{1}{2\delta}\frac{1}{\left[1+(\vartheta/2\delta)^2\right]^{3/2}}. \tag{8}$$

More layers of wires in the beam will result in a convolution of the successive angular distributions due to the individual layers, yielding a further broadening of the signal.

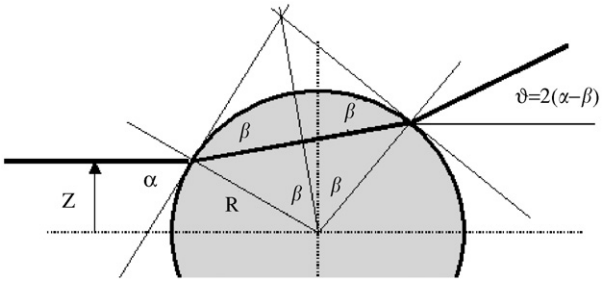

Fig. 1. Schematic neutron path refracted by a cylindrically shaped object.

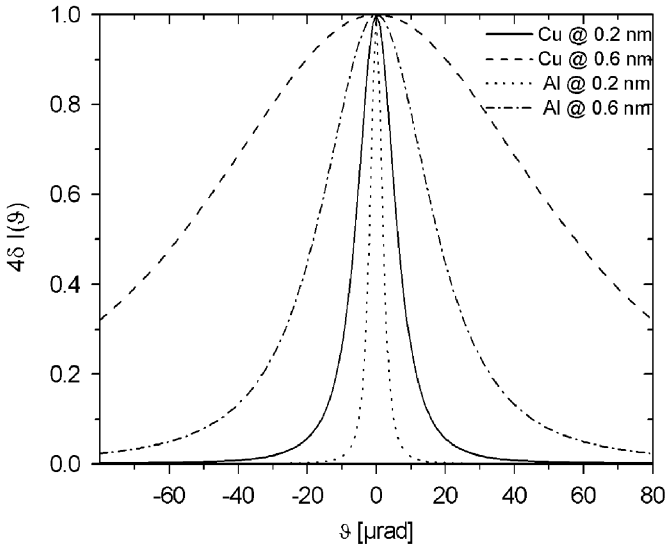

Fig. 2. Calculated normalised refractive angular distributions, $I(\vartheta)$, for a homogeneous neutron beam after refraction though Cu and Al wire for two distinct wavelengths of 0.2 and 0.6 nm.

For our calculations displayed in Fig. 2 we used $\rho_{Cu} = 8.4912 \times 10^{28}\,m^{-3}$, $\rho_{Al} = 6.0237 \times 10^{28}\,m^{-3}$, $\bar{b}_{Cu} = 7.718 \times 10^{-15}\,m$, $\bar{b}_{Al} = 3.449 \times 10^{-15}\,m$ and for a wavelength of 0.2 nm this means $\delta_{Cu} = 4.172 \times 10^{-6}$ and $\delta_{Al} = 1.323 \times 10^{-6}$.

2.2. Monochromatic SESANS/TOF SESANS

A typical SESANS arrangement, based on the spin-echo principle, [10,11] is sketched in Fig. 3. A polarised neutron beam enters the instrument that consists of two precession arms, with opposite magnetic induction B. Each arm consists of a parallelogram shaped region of length L and inclination angle θ_0, in which this induction is present. In the first arm a certain Larmor phase is generated. If the arrangement is in "spin-echo" the second arm will exactly compensate this precession phase for each trajectory. If we place a sample in the centre of the arrangement the compensation is disturbed because the scattered neutrons travel a different path through the magnetic field region in the second arm. This will cause a shift in Larmor precession phase for these neutrons. Hence the total beam, made up of a non-phase-shifted (un-scattered neutrons) and phase-shifted (scattered neutrons) part, will be depolarised. This depolarisation is a measure for small-angle scattering.

Because the inclination of the precession faces θ_0 is in the xz-plane, this arrangement is only sensitive to small-angle scattering in the xz-plane. This must be kept in mind for samples like wires, giving anisotropic scattering. In this case, the orientation of the wires becomes important.

The net Larmor precession $\varphi(\vartheta, B, \lambda)$ for a single neutron upon leaving the arrangement is given by

$$\varphi(\vartheta, B, \lambda) = cL\vartheta(z)B\lambda \cot\theta_0 \tag{9}$$

where ϑ (z) is the scattering angle and $c = 4.6368 \times 10^{14}\,T^{-1}\,m^{-2}$ is a universal constant. The polarisation $P(B, \lambda)$ of the scattered beam after the arrangement, reduced to the polarisation of the empty arrangement, is given by

$$P(B, \lambda) = \int_{-\pi/2}^{\pi/2} I(\vartheta)\cos(cL\vartheta B\lambda \cot\theta_0)\,d\vartheta. \tag{10}$$

Therefore, $P(B, \lambda)$ is essentially the Fourier transform of the function I(ϑ) found in Eq. (7). This implies that in the SESANS technique we measure a "real space signal". This simplifies the calculation for more than one layer of wires, because a convolution in Fourier space is a multiplication in real space. So

$$P(B, \lambda)_{n\_layers\_wire} = P(B, \lambda)^n. \tag{11}$$

Since both B and λ are contained in the argument of the cosine in Eq. (10), we can use either of these parameters as "scanning parameters". In the monochromatic SESANS we use B as scanning parameter and in the TOF SESANS we use λ as scanning parameter. Furthermore substitution of $I(\vartheta)$ in Eq. (10) yields

$$P(B, \lambda) = \int_0^{\infty} \frac{\cos(\kappa y)}{(1 + y^2)^{3/2}}\,dy, \tag{12}$$

where

$$\kappa = 2\delta cL \cot\theta_0 B\lambda \quad \text{and} \quad y = \frac{\vartheta}{2\delta}. \tag{13}$$

This Fourier transform can be evaluated as

$$P(B, \lambda) = \kappa K_1(\kappa) \tag{14}$$

where $K_1(x)$ is the first-order modified Bessel function of the second kind.

2.3. USANS

The ultra-high-resolution small-angle scattering double-crystal diffractometer is described in Ref. [8]. Using perfect silicon crystals a rocking curve is measured. Small-angle scattering will be observed as broadening of this rocking curve. The rocking curve is made by a stepwise rotation of the Si crystal analyser. The intensity is measured as a function of the scattering angle θ, or the scattering vector q, defined for small angles $q = 2\pi\theta/\lambda$.

The convolution of the normalised angular distribution $I(\vartheta)$ of Eq. (7), with the instrumental resolution, obtained from the normalised distribution $I(\vartheta)$ for the empty beam scan, enables us to compare the measured distribution observed by the instrument with theory.

3. Measurements

3.1. Sample

As samples we used commercial Cu and Al wire. The properties are summarised in Table 1. The layer of baked "enamelled" paint was not stripped and was not taken into account in the calculations. This (organic) layer is only several μm thick, hence a fraction of the total sample.

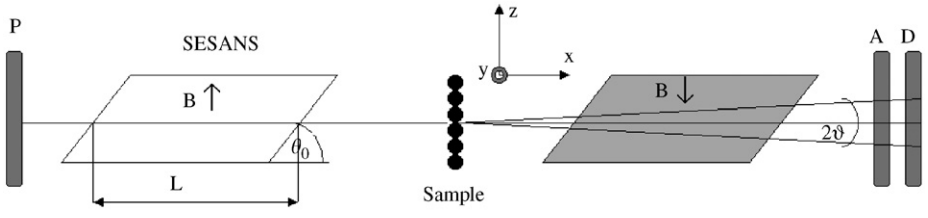

Fig. 3. Schematic SESANS arrangement with polariser (P), analyser (A) and detector (D). In the scheme of a monochromatic SESANS we add a monochromator in front of the polariser. For the TOF-SESANS instrument we add a chopper just behind the polarizer.

Table 1
Sample data

Sample #	Material	Diameter (mm)	Coating
1	Cu	1	Enamelled
2	Al	0.82	Enamelled
3	Cu	0.080	No coating
4	Cu	2	No coating

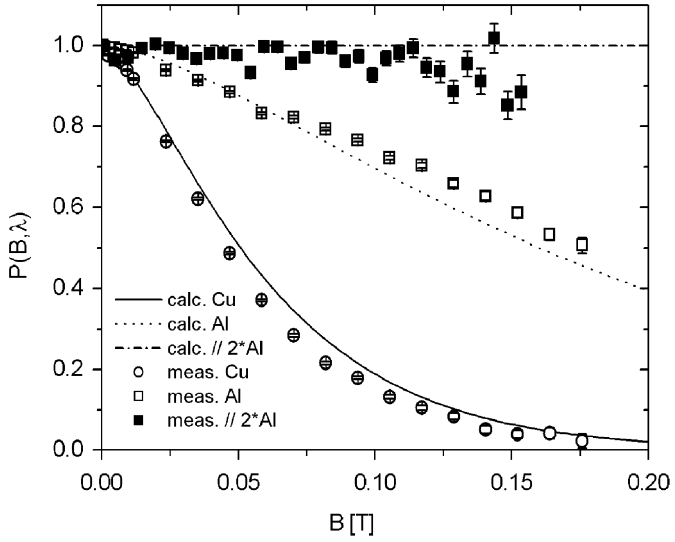

Fig. 4. Normalised polarisation, P (B,λ), as function of magnetic induction of the instrument and a constant wavelength. Top curve represents the calculation of two layers of Al wire with wires parallel to the sensitive direction together with the measurement (filled squares). Middle curve represents the calculation of one layer of Al wires together with measurement (open squares) and bottom curve represents the calculation of Cu together with the measurement (open circles). Middle and bottom curve represent wires perpendicular to the sensitive direction.

Because of this low fraction and its organic nature we only expect very low intensity of incoherent scattering into 4π and, therefore, no influence on the refraction effects of the Cu or Al. The samples consisted of one layer of wires with a negligible spacing in between. In one case we used two layers of Al wire. If not mentioned specifically the wires were orientated perpendicular to the sensitive direction of the instrument, i.e. with the axes in the y-direction as shown in Fig. 3.

3.2. Monochromatic SESANS

In Fig. 4 we give the results for samples #1 and #2 measured on monochromatic SESANS. The polarisation of the sample measurement is simply divided by the empty beam polarisation, which is basically the deconvolution of the measurement and the instrument, according to the remark preceding Eq. (11).

We see that the polarisation decreases as the magnetic induction, B, increases. The lines are the calculations according to Eq. (14) with Eq. (13). The measurements are in reasonable agreement with theory which contains no adjustable parameters. However, if we increase the value for $\bar{b}_{\mathrm{Cu}}$ by 7% and $\bar{b}_{\mathrm{Al}}$ by 10% we find a much better agreement. When the wire is parallel to the sensitive direction, the refraction occurs in the plane in which the instrument is insensitive for the small-angle scattering and, therefore, we see almost no effect. To enhance a possible small-angle scattering effect we used two layers of Al wire. Any isotropic small-angle scattering by inhomogenieties, surface roughness or oxide layer within our instrumental resolution would be observable in this geometry. There is some evidence of such scattering.

3.3. TOF SESANS

In the TOF mode the scanning parameter is the wavelength λ. Angular distribution of the beam caused by a sample will show up as depolarisation as function of λ.

In Fig. 5 we show the results for the Cu wires, #1, parallel to the sensitive direction of momentum transfer. No depolarisation is found at all. Hence no observable angular distribution by the wires is found. If we rotate the sample and measure the refraction we find a good agreement with the theory. Because scanning the parameter λ in our TOF-SESANS instrument gives a smaller measurement range as scanning B in the monochromatic SESANS, we observe less depolarisation due to refraction. Therefore, better agreement with the theory is found, as compared to that with monochromatic SESANS. Although the TOF-SESANS uses a larger wavelength, its measurement range is smaller because the parameter B is practically limited to 20% of the B in the monochromatic

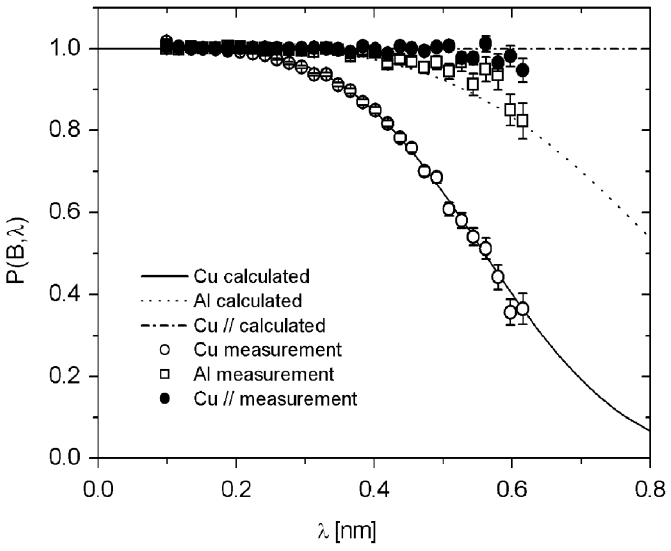

Fig. 5. Normalised polarisation, P (B,λ), as function of wavelength with a constant B. Top curve represents the calculation of Cu wire with the wires parallel to the sensitive direction together with the measurement (filled circles). Middle curve represents the calculation of one layer of Al wires together with measurement (open squares) and bottom curve represents the calculation of Cu together with the measurement (open circles). Middle and bottom curve represent wires perpendicular to the sensitive direction.

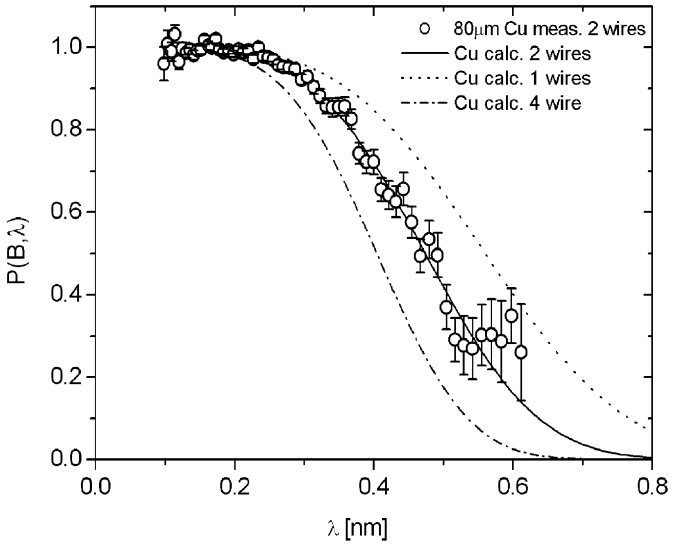

Fig. 6. The data points (open circles) represent the measured normalised polarisation, $P(B,\lambda)$, as function of wavelength and constant B for two layers of Cu wires of 80 μm diameter. The curves represent the calculation for 1 (dotted), 2 (solid) and 4 (dash–dot) layers of wire.

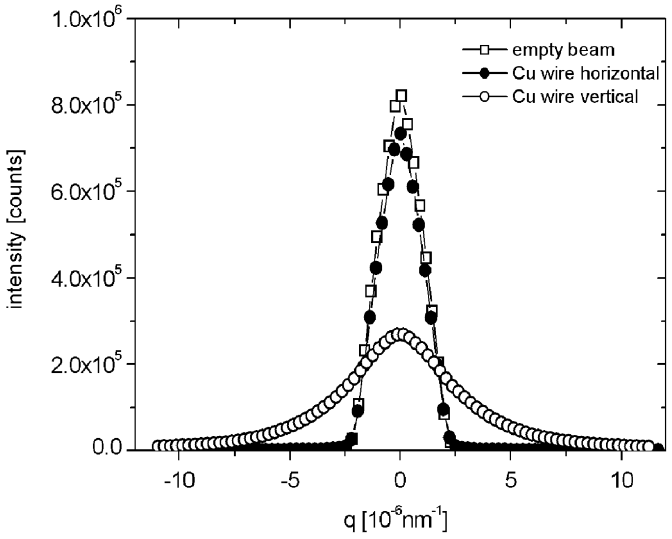

Fig. 7. Raw data from USANS measurement on neutron refraction by Cu wires. The empty beam measurement is represented by the open squares, the 'Cu wire horizontal' by the filled circles and the 'Cu wire vertical' by the open circles. The error bars are much smaller than the symbols.

SESANS; also $\cot\theta_0$ is practically limited to 10% of that of the monochromatic SESANS. This implies a smaller κ in Eq. (13). However, even with one layer of Al wires, #2, the refraction effect is still significant.

In the measurement, shown in Fig. 6, we used two layers of Cu wire (#3) instead of one. This illustrates the validity of Eq. (14) and the devastating effect of depolarisation produced by multiple wires in the beam for a spin-echo small-angle instrument. The figure shows that the measured depolarisation in (much smaller diameter) 80 μm Cu wires is also in good agreement with the theory. This confirms that Eq. (6) is independent of the wire diameter. Note that Eq. (6) using Snell's law is only valid if the coherence length of the (polarised) neutron in the instrument is much smaller than the diameter of the wire in the wire screen. The coherence length in this spin-echo arrangement is equal to the so-called spin-echo length. In this particular case of TOF-SESANS the maximum value is approximately 2 μm [5]. If the wire diameter comes close to this value, we would observe a periodic signal illustrating the periodic cross-section variation of the wire screen. For this limiting situation we can use the phase-object approximation, which is described by de Haan [12].

3.4. Usans

USANS measurements were taken with the empty beam, wires (#4) oriented vertically and (#4) horizontally. Data were collected in 20 s per data point with a q step size of $2.78\times10^{-7}\,\mathrm{nm}^{-1}$.

Fig. 7 shows the three data sets, without background correction. The empty beam shows a FWHM of around $2\times10^{-6}\,\mathrm{nm}^{-1}$. The scattering from the horizontally oriented

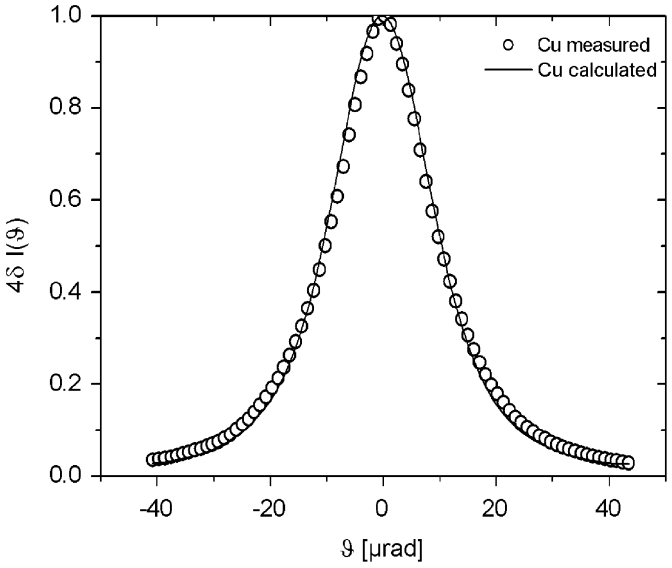

Fig. 8. The open circles represent the measurement of the vertical oriented Cu wire. The curve represents the calculation convoluted with the empty beam measurement.

wires correlates well with the empty data set after accounting for transmission loss. Refraction from wires oriented horizontally should not produce scattering in the horizontal sensitive direction of the instrument. This proves there is no observable SANS from the Cu itself by surface roughness or inhomogenieties in the Cu. The vertical orientation shows a clear broadening of the beam by refraction.

Fig. 8 shows the experimental data from vertical Cu wires (circles) and the theoretical curve (solid line) from Eq. (7), which was convoluted with the empty beam measurement. Agreement with theory is good.

4. Conclusion

We have measured and calculated the effect of refraction of cylindrical wires in a neutron beam. We have shown that the diameter of the wire is not important for the effect of refraction (as long as the diameter is much larger than the coherence length of the neutron in the instrument). We have shown that the effect can be significant and should be taken into account when designing an instrument or sample environment that is sensitive to ultra small-angle scattering. If there are more layers of wires involved or with instruments such as USANS and SESANS, the effect can be especially devastating. An alternative for cylindrical wires would be "ribbon"-shaped wires, already used in many NSE-spectrometers, which produce no angular redistribution after refraction. We have also shown that the more established instruments such as the USANS instrument at NIST and the monochromatic SESANS give a result complementarily to the prototype TOF-SESANS. This is a good demonstration that TOF-SESANS works and that it is becoming powerful tool to investigate ultra SANS. The TOF mode will become increasingly important for the SESANS technique because of the developments in new powerful spallation sources like the SNS, Oak Ridge, Tennessee, USA, and the second target station at ISIS, UK.

Acknowledgements

We would like to thank Theo Rekveldt and Wicher Kraan for several constructive discussions on this subject. Special thanks to Chris Duif for his assistance with the SESANS measurements. This work was financially supported by the Nederlandse Organisatie voor Wetenschappelijk Onderzoek (NWO). The USANS instrument at the NCNR is supported by the National Science Foundation under agreement DMR-9986442.

References

[1] R. Gahler, J. Kalus, W. Mampe, Phys. Rev. D 25 (11) (1982) 2887.
[2] S.M. Choi, J.G. Barker, C.J. Clinka, Y.T. Cheng, P.L. Gammel, J. Appl. Crystallogr. 33 (3) (2000) 793.
[3] M.T. Rekveldt, Physica B 350 (2004) 791.
[4] W.G. Bouwman, T.V. Krouglov, J. Plomp, S.V. Grigoriev, W.H. Kraan, M.T. Rekveldt, Phys. B-Condense. Matter 350 (1-3) (2004) 140.
[5] W.G. Bouwman, W. Stam, T.V. Krouglov, J. Plomp, S.V. Grigoriev, W.H. Kraan, M.T. Rekveldt, Nucl. Instr. Meth. A 529 (1–3) (2004) 16.
[6] J. Plomp, V.O. de Haan, R.M. Dalgliesh, S. Langridge, A.A. van Well, Physica B, 2007, in press doi:10.1016/j.physb.2007.02.043.
[7] J. Plomp, V.O. de Haan, R.M. Dalgliesh, S. Langridge, A.A. van Well, Thin Solid Films, 2007, in press doi:10.1016/j.tsf.2006.12.129.
[8] J.G. Barker, C.J. Glinka, J.J. Moyer, M.H. Kim, A.R. Drews, M. Agamalian, J. Appl. Crystallogr. 38 (2005) 1004.
[9] V.F. Sears, Neutron Opt. (1989).
[10] R. Pynn, M.R. Fitzsimmons, H. Fritzsche, M. Gierlings, J. Major, A. Jason, Rev. Sci. Instrum. 76 (5) (2005).
[11] M.T. Rekveldt, Physica B 276 (2000) 55.
[12] V.O. de Haan, J. Plomp, W.G. Bouwman, M. Trinker, M.T. Rekveldt, C. Duif, E. Jericha, H. Rauch, A.A. van Well, J. Appl. Crystallogr. 40 (2007) 151.